



Viscous flow in a soft valve

K. Park¹, A. Tixier², A. H. Christensen¹, S. F. Arnbjerg-Nielsen¹,
M. A. Zwieniecki^{2,†} and K. H. Jensen^{1,†}

¹Department of Physics, Technical University of Denmark, DK-2800 Kgs. Lyngby, Denmark

²Department of Plant Sciences, University of California, Davis, CA 95616, USA

(Received 23 August 2017; revised 29 September 2017; accepted 5 November 2017;
first published online 11 December 2017)

Fluid–structure interactions are ubiquitous in nature and technology. However, the systems are often so complex that numerical simulations or *ad hoc* assumptions must be used to gain insight into the details of the complex interactions between the fluid and solid mechanics. In this paper, we present experiments and theory on viscous flow in a simple bioinspired soft valve which illustrate essential features of interactions between hydrodynamic and elastic forces at low Reynolds numbers. The set-up comprises a sphere connected to a spring located inside a tapering cylindrical channel. The spring is aligned with the central axis of the channel and a pressure drop is applied across the sphere, thus forcing the liquid through the narrow gap between the sphere and the channel walls. The sphere's equilibrium position is determined by a balance between spring and hydrodynamic forces. Since the gap thickness changes with the sphere's position, the system has a pressure-dependent hydraulic resistance. This leads to a nonlinear relation between applied pressure and flow rate: flow initially increases with pressure, but decreases when the pressure exceeds a certain critical value as the gap closes. To rationalize these observations, we propose a mathematical model that reduced the complexity of the flow to a two-dimensional lubrication approximation. A closed-form expression for the pressure drop/flow rate is obtained which reveals that the flow rate Q depends on the pressure drop Δp , sphere radius a , gap thickness h_0 , and viscosity η as $Q \sim \eta^{-1} a^{1/2} h_0^{5/2} (1 - \Delta p / \Delta p_c)^{5/2} \Delta p$, where the critical pressure Δp_c scales with the spring constant k as $\Delta p_c \sim k h_0 a^{-2}$. These predictions compared favourably to the results of our experiments with no free parameters.

Key words: flow-structure interactions, lubrication theory, microfluidics

1. Introduction

Fluid flow in flexible geometries occurs in many biological, medical, and industrial environments (Duprat & Stone 2015). Systems that couple the elasticity of a solid

† Email addresses for correspondence: mzwienie@ucdavis.edu, khjensen@fysik.dtu.dk

body with the motion of a fluid often have interesting properties; for instance, interactions between fluid-mechanical and elastic forces can lead to nonlinear pressure-drop/flow-rate relations (Luo & Pedley 2000; Grotberg & Jensen 2004; Heil & Hazel 2015) and the generation of instabilities (Heil & Hazel 2011), even in relatively simple channel geometries.

Soft channels and valves play important roles in biological fluid systems: from flexible veins that carry nutrients in animals (Heil & Hazel 2011) to valves which maintain unidirectional flow through the human heart (Sotiropoulos, Le & Gilmanov 2016). Soft valves are also relevant to fluid transport in plants; for instance, in torus-margo pit pores, microscopic channels that permit water flow between neighbouring xylem tracheid conduits in coniferous trees (Choat, Cobb & Jansen 2008; Jensen *et al.* 2016). The pore structure prevents air embolisms from spreading inside the plant by blocking the pore with a circular disc if a large pressure difference develops between adjacent tracheids. The disc is held in place by soft cellulose fibres which can deform elastically. This soft geometry may modify flow even in the absence of air embolisms; however, previous studies have assumed either a static geometry (Lancashire & Ennos 2002; Schulte 2012) or inviscid flows (Chapman, Rand & Cooks 1977), and the effect of fluid–structure interactions at low Reynolds numbers on this system is not currently well understood.

Systems that couple the elasticity of a solid body with the motion of a fluid link two sets of dynamics that, even when treated separately, can be quite complicated. The properties of biological channels and valves have been studied extensively; however, the geometry is often so complex that numerical simulations or *ad hoc* assumptions must be used to gain insight into the details of the complex interactions between the fluid and solid mechanics (Bellhouse & Talbot 1969; McCulloh, Sperry & Adler 2003; Kim & Bush 2012; Park, Kim & Kim 2014; Yang *et al.* 2014; Gart *et al.* 2015; Jensen *et al.* 2016). Studies on model systems inspired by nature provide a promising alternative to *in vivo* experiments or full-scale numerical simulations. For instance, experiments on microfluidic devices have demonstrated that fluid-induced deformation of elastic sheets and fibres in channels can influence the flow at low Reynolds numbers (Wexler *et al.* 2013; Ledesma-Alonso, Guzmán & Zenit 2014), and similar results have been obtained using external mechanical actuation (Holmes *et al.* 2013).

In this paper, we present experiments and theory on a simple spring-actuated valve system inspired by biology. It captures many of the nonlinear interactions that characterize flow in soft geometries where the hydraulic resistance varies with applied pressure. The valve is suitable for regulation of small-scale fluid flows and relevant to several biofluid dynamics problems. Moreover, the simple geometry allows us to derive a closed-form solution, based on lubrication theory, which is compared to experimental data.

2. Experiment

We consider the effect of couplings between flow and elasticity on the idealized soft valve shown in figure 1(a): a sphere connected to an extension spring located inside a tapering cylindrical pipe. The spring is aligned with the central axis of the channel and a pressure drop Δp is applied across the sphere. The sphere's equilibrium position is determined by a balance between elastic and hydrodynamic forces. This leads to a nonlinear relation between applied pressure Δp and flow rate $Q = \Delta p/R(\Delta p)$, where $R(\Delta p)$ is the pressure-dependent hydraulic resistance.

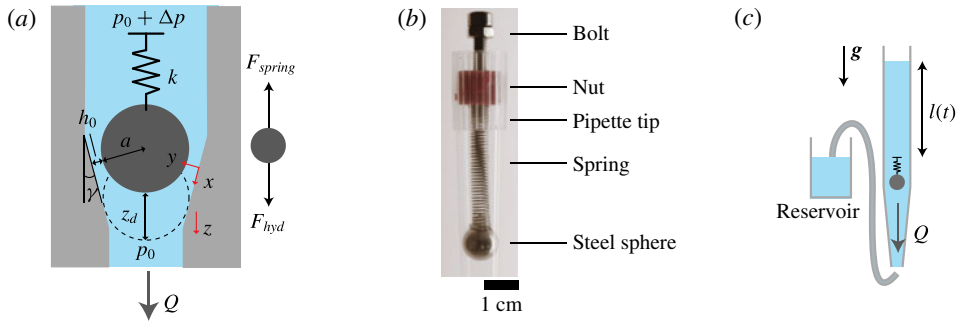


FIGURE 1. Schematics of the soft valve system and the experimental set-up. (a) Schematic of the spring-actuated soft valve. A sphere of radius a is suspended from a spring (spring constant k) inside a tapering channel. The sphere's position is determined by force equilibrium between the hydrodynamic and spring forces. (b) Photograph of the set-up showing the steel sphere, extension spring and pipette tip. (c) Schematic of the pressure-drop/flow-rate measurement system. The pressure drop is controlled by the liquid column height $l(t)$, and the flow rate $Q = \pi(D/2)^2 dl/dt$ and pressure drop $\Delta p = \rho gl(t)$ are determined by image analysis (see additional details in text).

2.1. Experimental methods

The valve was fabricated using a steel sphere of radius $a = 5$ mm and mass $m_{sphere} = 4 \times 10^{-3}$ kg (KVJ Aktieselskab, 45RB5) which was glued onto an extension spring (spring constant $k = 0.16$ N mm $^{-1}$, RS Components 821-273) (see figure 1b). The spring and sphere were anchored to a M4 bolt that allowed us to control the vertical position of the sphere along the central axis of a 3 mL pipette tip of opening angle $\gamma = 0.024$ rad (Alpha Laboratories, LW8930). Finally, both ends of the pipette were connected to silicone tubing (inner diameter $D = 12$ mm). We used the hydrostatic pressure difference provided by a vertical liquid column of height $l(t)$ in the silicone tubing to drive flow across the valve, thus sweeping a broad range of pressure drops Δp in each experiment (see figure 1c). The liquid column height $l(t)$ was tracked over time using image analysis of photographs captured using a digital camera (Canon, EOS 5D MARK III, 35 mm Sigma lens F1.4 DG HSM Art) as described in the Appendix. The pressure drop $\Delta p = \rho gl(t)$ and flow rate $Q = \pi(D/2)^2 dl/dt$ were subsequently determined, where ρ is the liquid density and g is the gravitational acceleration (see figure 1c). In the experiments, we varied the initial ball position in the range $z_d \sim 2.5$ – 4.5 mm (corresponding to initial gap thicknesses of $h_0 = z_d \sin \gamma \sim 60$ – 110 μ m), and the liquid viscosity from deionized (DI) water (1 cSt) to silicone oil (100 cSt).

2.2. Observations

Our experiments reveal that the flow rate increases linearly with pressure when the pressure drop is relatively small, because the position of the sphere is not influenced by the flow (figure 2). However, as pressure increases, hydrodynamic forces push the sphere towards the channel wall, thus reducing the gap size h_0 (see figure 1a). This leads to an increase in the resistance to flow. After reaching a maximum in flow Q_{max} , at the pressure Δp_{max} , the flow rate starts to decrease with increasing pressure and slowly approaches $Q = 0$ at the critical pressure drop Δp_c . The absolute magnitude of the flow can be tuned by varying the initial ball position z_d (and hence the thickness of

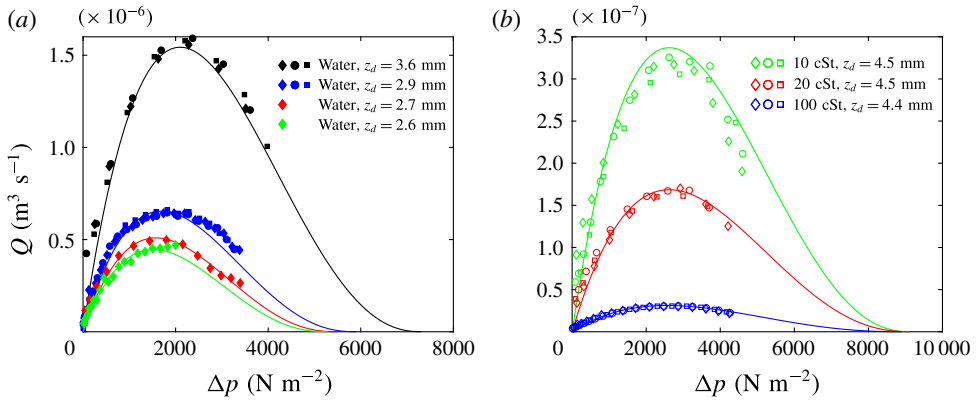


FIGURE 2. Pressure-drop/flow-rate relation for viscous flow in a soft valve. (a) Flow rate Q plotted as a function of applied pressure Δp for DI water flow with viscosity $\eta = 1 \text{ cSt}$, spring constant $k = 0.16 \text{ N mm}^{-1}$, and sphere radius $a = 5 \text{ mm}$. Results for initial ball position $z_d = 2.6, 2.7, 2.9$ and 3.6 mm are shown as green, red, blue and black symbols, respectively. Maximum Reynolds number in each case is $\sim 13, 16, 19$ and 48 , respectively. (b) Flow rate Q plotted as a function of applied pressure Δp for silicone oil with initial ball position $z_d \sim 4.5 \text{ mm}$, spring constant $k = 0.16 \text{ N mm}^{-1}$, and sphere radius $a = 5 \text{ mm}$. Results for viscosities $\eta = 10, 20$ and 100 cSt are shown as green, red and blue symbols, respectively. Maximum Reynolds number in each case is $\sim 1, 0.24$ and 0.008 , respectively.

the gap between the sphere and tapering channel walls) or by changing the viscosity η of the fluid. We observe that both the peak flow rate Q_{max} and optimum pressure Δp_{max} increase with z_d . By contrast, only the flow rate Q appears to be affected significantly by variations in viscosity η . We note that the observed pressure-drop/flow-rate relation is similar to that of flows through externally pressurized elastic tubes (Luo & Pedley 2000).

The focus of our paper is on predicting the flow rate as a function of the system parameters. The Reynolds number $Re = \rho u_{gap} h_0 / \eta = (\rho Q) / (2\pi \eta a) \leq 10$ in most our experiments, and hence viscous effects dominate the flow. Here, $u_{gap} = Q / (2\pi a h_0)$ is the characteristic flow speed in the gap. We take advantage of the low-Reynolds-number conditions by using steady-state lubrication theory in the following analysis. However, we note that in experiments conducted with water at or above Reynolds number $Re_c \simeq 30$, periodic oscillations of the sphere's vertical position and flow rate were observed. For instance, in a $Re \simeq 30$ experiment with initial ball displacement $z_d = 3.6 \text{ mm}$ and pressure drop in the range $\Delta p \sim 3500\text{--}5000 \text{ Pa}$, we observed periodic disturbances with a frequency of $f_{osc} = 2.7 \text{ Hz}$ (see figure 5 in the Appendix and Supplementary movie 2 available at <https://doi.org/10.1017/jfm.2017.805>). This pattern has features that resemble self-excited oscillations found in other elastic flow systems (see e.g. Luo & Pedley 1996). In our system, the onset of oscillation and their detailed pattern are influenced by a number of effects; including hydrodynamic instabilities in the flow, the coupling between the flow and the spring–sphere system, as well as the dual relationship between flow rate Q and pressure drop Δp . We note first that the natural frequency of the spring–steel sphere system with moving water column $f_{spring} = (2\pi)^{-1} (k / (m_{sphere} + m_{water}))^{1/2} \sim 6 \text{ Hz}$ in approximate agreement with the observed signal, where m_{water} is the mass of the fluid column above and below

the valve (~ 0.1 kg). The motion of the sphere is, moreover, in rough accord with the sphere's vortex shedding frequency $f_v = St u_{gap}/(2a) = St Re v/(2ah_0) = 3$ Hz, computed with values of $St = 0.1$ for the Strouhal number (see e.g. Bearman 1984; Williamson 1996; Williamson & Govardhan 2004), $Re = 30$, $a = 5$ mm, $h_0 = 0.1$ mm and $v = \eta/\rho = 10^{-6}$ m²s⁻¹. This may indicate that vortex shedding is an important factor in determining the characteristics of the oscillations. However, the onset of this instability is also influenced by the blockage ratio $h_0/(2a)$. For instance, Sahin & Owens (2004) and Patil & Tiwari (2008) found that the critical Reynolds number Re_c for the onset of oscillations decreases with increasing blockage ratio. Finally, we note that the pressure could vary back and forth if a constant flow rate is maintained through the system. This may affect the characteristics of the periodic motion since the pressure drop Δp is a multivalued function of flow rate Q .

3. Theory

To rationalize the experimental observations (figure 2), we seek to characterize the pressure-drop/flow-rate relation as a function of the system parameters

$$Q = \frac{\Delta p}{R}. \tag{3.1}$$

The pressure-dependent hydraulic resistance $R(\Delta p)$ is a function of the vertical position z of the sphere, which in turn is determined by the force balance on the sphere due to the spring and hydrodynamics forces along the z -axis (see figure 1a):

$$F_{spring} + F_{hyd} = 0. \tag{3.2}$$

We proceed in two steps to compute the pressure-dependent resistance R in (3.1): First, we use lubrication theory to determine the flow field in the narrow gap between the sphere and the tapering channel walls for a fixed vertical position of the sphere and pressure drop Δp . This leads to a position-dependent hydraulic resistance $R(z)$. Our analysis of the static problem follows Smistrup & Stone (2007), who considered a magnetically actuated ball valve. Then, we use the force-balance equation (3.2) to solve for the equilibrium position $z_{eq}(\Delta p)$, which leads to an expression for $R(\Delta p)$.

The valve system comprises a sphere connected to a spring in a tapering cylindrical channel with opening angle γ (see figure 1a). In the experiments, the sphere radius is $a = 5 \times 10^{-3}$ m while the typical size of the gap between the sphere and the channel walls is $h_0 \leq 10^{-4}$ m. We therefore consider the limit where the gap is narrow ($h_0 \ll a$), and let βa denote the vertical displacement of the sphere above the point of contact where $h_0 = 0$ and $\beta = 0$. The gap thickness can then be expressed in terms of β , the sphere radius a , and the opening angle γ as $h_0 = a\beta \sin(\gamma)$. Because the gap is narrow, the coordinate system can locally be considered as Cartesian, with x - and y -axes indicated in figure 1(a). Note that the z -axis in the diagram does not belong to this coordinate system.

3.1. Lubrication theory

The flow is governed by the Navier–Stokes and continuity equations

$$\rho \left[\frac{\partial \mathbf{u}}{\partial t} + (\mathbf{u} \cdot \nabla) \mathbf{u} \right] = -\nabla p + \eta \nabla^2 \mathbf{u}, \tag{3.3}$$

$$\nabla \cdot \mathbf{u} = 0, \tag{3.4}$$

where ρ denotes the density, η the viscosity, p the pressure, and \mathbf{u} the velocity field. In the steady low-Reynolds-number limit, the Navier–Stokes and continuity equations for the flow in the narrow gap ($h_0/a \ll 1$) reduce to the lubrication equations

$$\eta \frac{\partial^2 u_x}{\partial y^2} = \frac{\partial p}{\partial x}, \tag{3.5a}$$

$$0 = \frac{\partial p}{\partial y}, \tag{3.5b}$$

$$\frac{\partial u_x}{\partial x} + \frac{\partial u_y}{\partial y} = 0. \tag{3.5c}$$

From equation (3.5b) it is seen that the pressure does not depend on y , and hence u_x can be found from equation (3.5a), by using no-slip boundary conditions at $y = 0$ and $y = h(x)$, as

$$u_x(x, y) = \frac{1}{2\eta} \frac{\partial p}{\partial x} (y^2 - yh(x)). \tag{3.6}$$

The gap $h(x)$ between the sphere and the channel walls is locally approximated by a parabola

$$h(x) = h_0 \left[1 + \frac{x^2}{2h_0 a} + O\left(\frac{x^4}{h_0 a^3}\right) \right]. \tag{3.7}$$

The total flow rate, Q , is found by integrating the flow field (3.6) in the gap around sphere:

$$Q = 2\pi a \cos(\gamma) \int_0^{h(x)} u_x(x, y) dy = -\frac{\partial p}{\partial x} \frac{\pi a \cos(\gamma) h^3(x)}{6\eta}, \tag{3.8}$$

where the factor $2\pi a \cos(\gamma)$ comes from integrating along the circular gap of radius $a \cos(\gamma)$. Since the flow rate must be independent of x , the pressure drop across the sphere is

$$\Delta p = \int_{-\infty}^{\infty} \frac{\partial p}{\partial x} dx = \frac{6\eta Q}{\pi a \cos(\gamma)} \int_{-\infty}^{\infty} \frac{1}{h^3(x)} dx \tag{3.9a}$$

$$= \frac{9\eta Q}{2\sqrt{2} \cos(\gamma) (ah_0^5)^{1/2}} \tag{3.9b}$$

$$= \frac{9\eta Q}{2\sqrt{2} a^3 \cos \gamma (\beta \sin \gamma)^{5/2}}, \tag{3.9c}$$

where we have used that the gap size can be written as $h_0 = \beta a \sin(\gamma)$ in the final step. Note that the hydraulic resistance $R = \Delta p/Q$ scales with the gap viscosity, thickness and sphere radius as $R \sim \eta a^{-1/2} h_0^{-5/2}$.

3.2. Force balance

To derive the flow-rate/pressure-drop relation for the system, we proceed to determine the equilibrium position $z_{d,eq}$ of the sphere from the force balance (3.2) (see figure 1a). This leads to an expression for the equilibrium relative displacement $\beta_{eq} = z_{eq}/a$ which then used in (3.9c) to determine the resistance.

To model the extension spring we assume a linear spring force of

$$F_{spring} = -k\Delta z, \tag{3.10}$$

Viscous flow in a soft valve

where k is the spring constant and Δz is the vertical displacement from the equilibrium position. Let z_0 be the equilibrium length when no pressure is applied and let z_{max} be the maximum extension of the spring, obtained when the sphere touches the inclined wall. For a sphere located a distance $z_d = \beta a$ above the contact point, the spring extension is $\Delta z = z_{max} - z_0 - \beta a$, and hence the spring force is given by $F_{spring} = -k(z_{max} - z_0 - \beta a)$.

The hydrodynamic force on the sphere is given by

$$F_{hyd,i} = \int_{\partial\Omega} [-p\delta_{ij} + \eta(\partial_i u_j + \partial_j u_i)] n_j da, \quad (3.11)$$

where we use the index notation and $\partial\Omega$ denotes the surface of the sphere. In the lubrication limit, we expect that the pressure term dominates the vertical force on the sphere. The main pressure gradient occurs in a narrow region near the gap, and the pressure force can thus be approximated by assuming constant pressures above ($p_0 + \Delta p$) and below (p_0) the sphere:

$$\begin{aligned} F_{hyd}^{(p)} &\simeq 2\pi a^2(p_0 + \Delta p) \int_0^{\pi/2+\gamma} \cos(\theta) \sin(\theta) d\theta + 2\pi a^2 p_0 \int_{\pi/2+\gamma}^{\pi} \cos(\theta) \sin(\theta) d\theta \\ &= \pi a^2 \cos(\gamma)^2 \Delta p, \end{aligned} \quad (3.12)$$

where θ is the angle measured from the vertical. To obtain the viscous force, we note that in the lubrication approximation $\partial/\partial x \ll \partial/\partial y$, so the dominant term is

$$F_{hyd}^{(visc)} \simeq 2\pi a \cos(\gamma) \eta \int_{-\infty}^{\infty} \frac{\partial u_x}{\partial y} \Big|_{y=h(x)} \cos(\gamma) dx = \frac{4\pi}{3} \cos^2(\gamma) \sin(\gamma) \beta a^2 \Delta p, \quad (3.13)$$

where the prefactor $2\pi a \cos \gamma$ comes from integration around the contact line, and the factor $\cos \gamma$ in the integral from the force projection along the z -axis. Comparing the magnitude of the pressure (3.12) and viscous (3.13) forces, we find

$$\frac{F_{hyd}^{(visc)}}{F_{hyd}^{(p)}} = \frac{4}{3} \frac{h_0}{a}. \quad (3.14)$$

In our case, where $h_0 \ll a$, the pressure force is seen to dominate the hydrodynamic force on the sphere.

To find the vertical equilibrium position of the sphere, we now combine the spring force (3.10) and the pressure force (3.12) using the force-balance equation (3.2), and find

$$\pi a^2 \cos(\gamma)^2 \Delta p - k(z_d - a\beta) = 0, \quad (3.15)$$

where we have written the initial height as $z_d = z_0 - z_{max}$. This leads to an expression for the relative position β at equilibrium:

$$\beta = \frac{kz_d - \Delta p \pi a^2 \cos(\gamma)^2}{ka}. \quad (3.16)$$

Combining (3.16) and (3.9c) leads to a nonlinear pressure-dependent flow rate Q

$$Q = \frac{2\sqrt{2} \cos^6(\gamma) a^3}{9 \eta} \left(\frac{a\pi \sin(\gamma)}{k} \right)^{5/2} \left(\frac{kz_d}{\pi a^2 \cos^2(\gamma)} - \Delta p \right)^{5/2} \Delta p. \quad (3.17)$$

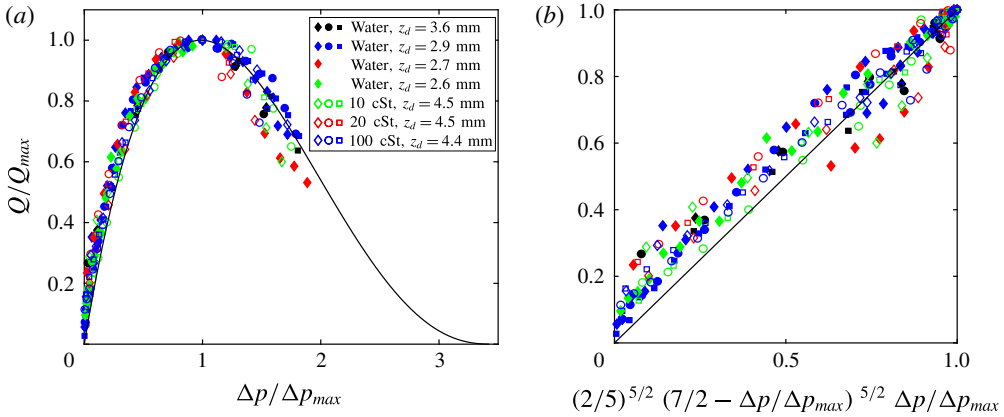


FIGURE 3. Normalized flow rate Q/Q_{max} plotted as a function of (a) relative pressure drop $\Delta p/\Delta p_{max}$ and (b) $(2/5)^{5/2}(7/2 - \Delta p/\Delta p_{max})^{5/2} \Delta p/\Delta p_{max}$, using data from figure 2(a,b). The solid line shows the theoretical prediction obtained using lubrication theory (3.21).

Introducing the low-pressure-limit resistance

$$R_0 = \frac{9}{2\sqrt{2} \sin(\gamma)^{5/2} \cos(\gamma)} \frac{\eta}{(az_d^5)^{1/2}} \tag{3.18}$$

and the critical pressure drop Δp_c that makes the ball block the channel

$$\Delta p_c = \frac{kz_d}{\pi a^2 \cos^2(\gamma)}, \tag{3.19}$$

leads to a convenient expression for the flow rate:

$$Q = \frac{\Delta p}{R_0} (1 - \Delta p/\Delta p_c)^{5/2}. \tag{3.20}$$

When $\Delta p \ll \Delta p_c$ the flow rate scales linearly with pressure drop Δp , in accord with experimental observations (figure 2). A maximum in the flow rate occurs at the pressure drop $\Delta p_{max} = 2/7 \Delta p_c$, above which the valve gradually closes and the flow rate Q starts to decay.

3.3. Comparison between experiment and theory

The lubrication-theory model for the flow rate Q (3.17) captures the essential qualitative behaviour of the experimental data (figure 2), and we find good quantitative agreement between experiments and theory with no free parameters. Moreover, the data collapsed onto a single line when scaled according to the maximum flow rate Q_{max} and corresponding pressure Δp_{max} (figure 3). The data collapse is seen to be in good accord with the prediction from (3.20), which yields

$$\frac{Q}{Q_{max}} = \left(\frac{\Delta p_c - \Delta p}{\Delta p_c - \Delta p_{max}} \right)^{5/2} \frac{\Delta p}{\Delta p_{max}} = \left(\frac{2}{5} \right)^{5/2} \left(\frac{7}{2} - \frac{\Delta p}{\Delta p_{max}} \right)^{5/2} \frac{\Delta p}{\Delta p_{max}}, \tag{3.21}$$

where we have used that the maximum pressure is $\Delta p_{max} = (2/7) \Delta p_c$.

3.4. Implications for biological soft valves

Elastic conduits and flexible valves are found in numerous biological fluid systems. Our geometry is qualitatively similar to torus-margo pits, microscopic channels that link neighbouring vascular channels in coniferous trees (Choat *et al.* 2008; Jensen *et al.* 2016). In these pores, an oblate spheroid is suspended from numerous flexible cellulose fibres above a narrow hole. Despite the difference in geometry, it is probable that the flow-rate/pressure-drop relation of these structures is qualitatively to our experiments (figure 2, (3.20)).

Elastic and geometric properties of pit pores were obtained by Capron *et al.* (2014), who found values of $z_d = 2 \mu\text{m}$, $a = 3.5 \mu\text{m}$, and $k \simeq 10 \text{ N m}^{-1}$. With these values, our theory predict a critical pressure for closing the valve of $\Delta p_c \sim 0.5 \text{ MPa}$, while the maximum flow is obtained at $\Delta p_{max} \sim 0.15 \text{ MPa}$.

4. Discussion and conclusion

In this paper we have presented an experimental and theoretical study of a bioinspired soft valve. The model system comprised a sphere connected to a spring located inside a tapering channel. A coupling between elasticity and fluid motion determines the hydraulic resistance of the valve because the position of the sphere is influenced by the flow, and *vice versa*. Using a simple set-up, we performed experiments to characterize the pressure-drop/flow-rate relationship for the system. Our data revealed a strongly nonlinear behaviour and the existence of an optimal pressure drop for the system where the flow rate is maximized.

Assuming low-Reynolds-number flow, we proposed a mathematical model that reduced the complexity of the flow to a two-dimensional lubrication approximation. The model revealed a relatively complete picture of the geometric and material parameters that affect flow through the system. The model predictions compared favourably to the results of our experiments. Our analysis is limited to steady viscous flows, though preliminary observations demonstrate the onset of self-excited oscillations.

Acknowledgements

This work was supported by a research grant (13166) from VILLUM FONDEN. We also thank P. E. Andersen, D. Shacham and E. Hansen for assistance in the design of the experimental set-up.

Supplementary movies

Supplementary movies are available at <https://doi.org/10.1017/jfm.2017.805>.

Appendix. Tracing the meniscus

The pressure-drop/flow-rate relation was determined experimentally as outlined in figures 1(c) and 4. A stack of images showing the meniscus movement was converted to grey scale and cropped to show the silicone tube above the soft valve. The two-dimensional images $I(z, x, t)$ were converted to a one-dimensional intensity profile $I'(z, t) = \sum_x I(z, x, t)$ by summing the values in each horizontal image row. We traced the position of the meniscus by locating the maximum in the intensity gradient $\sim \partial_z I'(z, t)$ at the position $z_{max}(t)$. This yielded the meniscus position $z_{max} = l(t)$, which in turn allowed us to determine the flow rate Q . In order to minimize effects of image

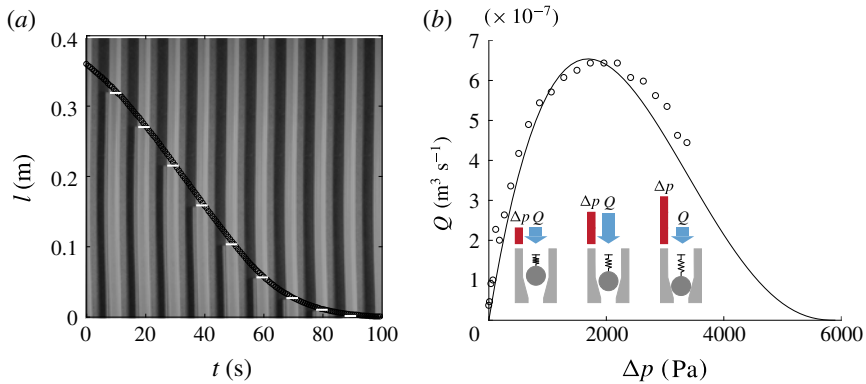


FIGURE 4. Experimental result for $z_d = 2.9$ mm with water. (a) Time versus liquid column height graph with a montage of images of every 10 s. Tracking points (circles) are well fitted with experimental images (horizontal white lines). (b) Pressure-drop and flow-rate graph from (a). Inset shows the ball position at a certain pressure drop.

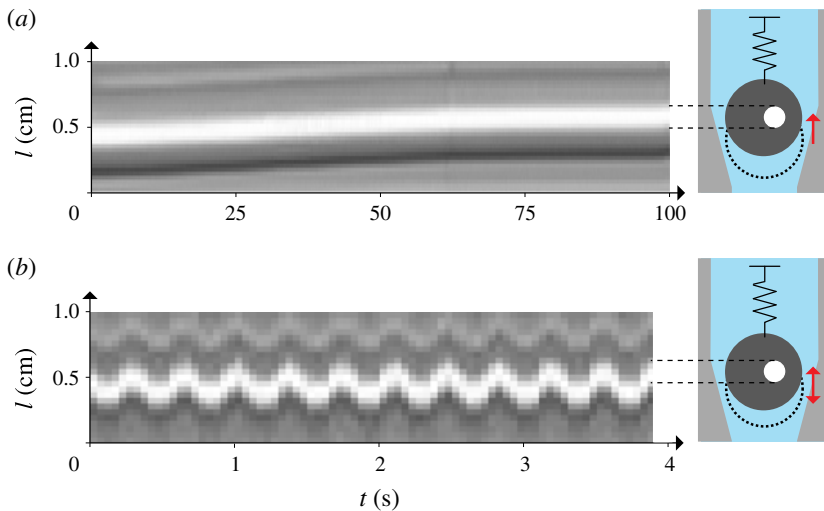


FIGURE 5. (a) Experimental kymograph of a soft valve with water and $z_d = 2.9$ mm. Image variation shows ball movement during the experiment (see Supplementary movie 1). (b) Kymograph of a soft valve with water and $z_d = 3.6$ mm for the first 4 s of Supplementary movie 2. The pressure drop decreases from 4800 to 4500 Pa and the corresponding Reynolds number is ~ 30 . The observed oscillation frequency $f_{\text{obs}} \sim 2.7$ Hz. See also Supplementary movie 2.

noise in determining z_{max} , we manually indicated the initial meniscus position and used a tracing window.

References

- BEARMAN, P. W. 1984 Vortex shedding from oscillating bluff bodies. *Annu. Rev. Fluid Mech.* **16** (1), 195–222.
- BELLHOUSE, B. J. & TALBOT, L. 1969 The fluid mechanics of the aortic valve. *J. Fluid Mech.* **35** (4), 721–735.

- CAPRON, M., TORDJEMAN, P., CHARRU, F., BADEL, E. & COCHARD, H. 2014 Gas flow in plant microfluidic networks controlled by capillary valves. *Phys. Rev. E* **89** (3), 033019.
- CHAPMAN, D. C., RAND, R. H. & COOKS, J. R. 1977 A hydrodynamical model of bordered pits in conifer tracheids. *J. Theor. Biol.* **67** (1), 11–24.
- CHOAT, B., COBB, A. R. & JANSEN, S. 2008 Structure and function of bordered pits: new discoveries and impacts on whole-plant hydraulic function. *New Phytol.* **177** (3), 608–626.
- DUPRAT, C. & STONE, H. A. 2015 *Fluid-Structure Interactions in Low-Reynolds-Number Flows*. Royal Society of Chemistry.
- GART, S., SOCHA, J. J., VLACHOS, P. P. & JUNG, S. 2015 Dogs lap using acceleration-driven open pumping. *Proc. Natl Acad. Sci. USA* **112** (52), 15798–15802.
- GROTBERG, J. B. & JENSEN, O. E. 2004 Biofluid mechanics in flexible tubes. *Annu. Rev. Fluid Mech.* **36**, 121–147.
- HEIL, M. & HAZEL, A. L. 2011 Fluid-structure interaction in internal physiological flows. *Annu. Rev. Fluid Mech.* **43**, 141–162.
- HEIL, M. & HAZEL, A. L. 2015 Flow in flexible/collapsible tubes. In *Fluid-Structure Interactions in Low-Reynolds-Number Flows* (ed. C. Duprat & H. Stone), pp. 280–312. Royal Society of Chemistry.
- HOLMES, D. P., TAVAKOL, B., FROEHLICHER, G. & STONE, H. A. 2013 Control and manipulation of microfluidic flow via elastic deformations. *Soft Matt.* **9** (29), 7049–7053.
- JENSEN, K. H., BERG-SØRENSEN, K., BRUUS, H., HOLBROOK, N. M., LIESCHE, J., SCHULZ, A., ZWIENIECKI, M. A. & BOHR, T. 2016 Sap flow and sugar transport in plants. *Rev. Mod. Phys.* **88** (3), 035007.
- KIM, W. & BUSH, J. W. M. 2012 Natural drinking strategies. *J. Fluid Mech.* **705**, 7–25.
- LANCASHIRE, J. R. & ENNOS, A. R. 2002 Modelling the hydrodynamic resistance of bordered pits. *J. Expl. Bot.* **53** (373), 1485–1493.
- LEDESMA-ALONSO, R., GUZMÁN, J. E. V. & ZENIT, R. 2014 Experimental study of a model valve with flexible leaflets in a pulsatile flow. *J. Fluid Mech.* **739**, 338–362.
- LUO, X. Y. & PEDLEY, T. J. 1996 A numerical simulation of unsteady flow in a two-dimensional collapsible channel. *J. Fluid Mech.* **314**, 191–225.
- LUO, X. Y. & PEDLEY, T. J. 2000 Multiple solutions and flow limitation in collapsible channel flows. *J. Fluid Mech.* **420**, 301–324.
- MCCULLOH, K. A., SPERRY, J. S. & ADLER, F. R. 2003 Water transport in plants obeys Murray's law. *Nature* **421** (6926), 939–942.
- PARK, K., KIM, W. & KIM, H.-Y. 2014 Optimal lamellar arrangement in fish gills. *Proc. Natl Acad. Sci. USA* **111** (22), 8067–8070.
- PATIL, P. P. & TIWARI, S. 2008 Effect of blockage ratio on wake transition for flow past square cylinder. *Fluid Dyn. Res.* **40** (11), 753–778.
- SAHIN, M. & OWENS, R. G. 2004 A numerical investigation of wall effects up to high blockage ratios on two-dimensional flow past a confined circular cylinder. *Phys. Fluids* **16** (5), 1305–1320.
- SCHULTE, P. J. 2012 Computational fluid dynamics models of conifer bordered pits show how pit structure affects flow. *New Phytol.* **193** (3), 721–729.
- SMISTRUP, K. & STONE, H. A. 2007 A magnetically actuated ball valve applicable for small-scale fluid flows. *Phys. Fluids* **19** (6), 063101.
- SOTIROPOULOS, F., LE, T. B. & GILMANOV, A. 2016 Fluid mechanics of heart valves and their replacements. *Annu. Rev. Fluid Mech.* **48**, 259–283.
- WEXLER, J. S., TRINH, P. H., BERTHET, H., QUENNOUZ, N., DU ROURE, O., HUPPERT, H. E., LINDNER, A. & STONE, H. A. 2013 Bending of elastic fibres in viscous flows: the influence of confinement. *J. Fluid Mech.* **720**, 517–544.
- WILLIAMSON, C. H. 1996 Vortex dynamics in the cylinder wake. *Annu. Rev. Fluid Mech.* **28** (1), 477–539.
- WILLIAMSON, C. H. K. & GOVARDHAN, R. 2004 Vortex-induced vibrations. *Annu. Rev. Fluid Mech.* **36**, 413–455.
- YANG, P. J., PHAM, J., CHOO, J. & HU, D. L. 2014 Duration of urination does not change with body size. *Proc. Natl Acad. Sci. USA* **111** (33), 11932–11937.